MRI Cine-Tagging of Cardiac-Induced Motion for Noninvasive Staging of Liver Fibrosis

Thierry Lefebvre,[1,2,3] (iD) Léonie Petitclerc, MSc,[1,2,4] Mélanie Hébert,[1,2] Laurent Bilodeau, MD,[1,2]

Giada Sebastiani, MD,[5] Damien Olivié, MD,[1] Zu-Hua Gao, MD, PhD,[6]

Marie-Pierre Sylvestre, PhD,[2,7] Guy Cloutier, PhD, Eng,[1,8,9] Bich N. Nguyen, MD,[10]

Guillaume Gilbert, PhD,[1,11] and An Tang, MD, MSc[1,2,8]*

Background: MR elastography is a noninvasive technique that provides high diagnostic accuracy for the staging of liver fibrosis; however, it requires external hardware and mainly assesses the right lobe.

Purpose: To evaluate the diagnostic performance of MRI cine-tagging for staging fibrosis in the left liver lobe, using biopsy as the reference standard.

Study Type: Institutional Review Board (IRB)-approved two-center prospective study.

Population: Seventy-six patients with chronic liver disease who underwent an MRI cine-tagging examination and a liver biopsy within a 6-week interval.

Field Strength/Sequence: 2D-GRE multislice sequence at 3.0T with spatial modulation of the magnetization preparation sequence and peripheral pulse-wave triggering on two coronal slices chosen underneath the heart apex to capture maximal deformation with consecutive breath-holds adapted to patient cardiac frequency.

Assessment: A region of interest was selected in the liver close to the heart apex. Maximal strain was evaluated with the harmonic phase (HARP) technique.

Statistical Tests: Spearman's correlation, Kruskal–Wallis test, Mann–Whitney U-test, and receiver operating characteristic (ROC) analysis were performed.

Results: Liver strain measured on tagged images decreased with higher histological fibrosis stage ($\rho = -0.68$, $P < 0.0001$). Strain values were significantly different between all fibrosis stages ($P < 0.0001$), and between groups of fibrosis stages ≤F3 vs. F4 ($P < 0.05$). Areas under the ROC curves were 0.95 (95% confidence interval: 0.89–1.00) to distinguish fibrosis stages F0 vs. F4, 0.81 (0.70–0.92) for stages F0 vs. ≥F1, 0.84 (0.76–0.93) for stages ≤F1 vs. ≥F2, 0.86 (0.78–0.94) for stages ≤F2 vs. ≥F3, and 0.87 (0.77–0.96) for stages ≤F3 vs. F4.

Data Conclusion: MRI cine-tagging is a promising technique for measuring liver strain without additional elastography hardware. It could be used to assess the left liver lobe as a complement to current techniques assessing the right lobe.

Level of Evidence: 1
Technical Efficacy: 3

CHRONIC LIVER DISEASE (CLD) is characterized by the formation of liver fibrosis, a scarring process, which may lead to cirrhosis and potentially to liver failure.[1,2]

Because of the high prevalence of CLD, the burden of liver fibrosis is of great concern for the healthcare system.[3] The prevalence of CLD is currently on the rise, in part because of

the increase in nonalcoholic fatty liver disease (NAFLD) in parallel with the diabetes and obesity epidemics.[4] While liver biopsy remains the most widely accepted reference standard for staging hepatic fibrosis,[5] this observer-dependant technique is invasive and thus suboptimal for monitoring, thus prompting research on noninvasive approaches as alternatives.

Over the past two decades, numerous elastography methods relying on hepatic mechanical properties have been proposed for staging liver fibrosis, currently providing the highest diagnostic performance of available noninvasive techniques.[6] Several ultrasound (US)-based elastography methods, such as 1D transient elastography, point shear-wave elastography, and 2D shear-wave elastography, have been introduced clinically for this purpose. US-based techniques are fast, portable, and inexpensive; however, these techniques only cover a small sample area, yield high rates of uninterpretable results,[7] and have limited use in patients with obesity, narrow intercostal spaces, or ascites.[8] In parallel, magnetic resonance elastography (MRE), relying on an external mechanical driver system for wave generation, has been developed to assess liver stiffness.[9] MRE can be performed in obese patients and samples a larger region of the liver than US-based techniques. However, MRE can be challenging to perform in subjects with iron overload, especially at higher field strengths,[10] and requires extra hardware and postprocessing.[11] Furthermore, MRE techniques predominantly assess the right liver lobe, as the vibration source overlies this structure.[8]

Alternatively, liver deformation induced by cardiac motion can be assessed with MRI cine-tagging. This method, initially developed for cardiac imaging,[12] uses a magnetization grid (or "tags") to track the underlying tissue deformation without extra hardware. Recent studies have assessed liver fibrosis using the tagging method with different postprocessing analyses, including bending energy measurement,[13] Gabor filter,[14–16] harmonic phase (HARP) analysis,[17] and strain-encoded MRI, the latter method measuring strain without the need for tagged images.[18] Among these, the HARP postprocessing technique has stood out for its fast and automated analysis of tagged images, providing a measure of strain at each point of the liver.[19] Most previous studies have compared normal volunteers to cirrhotic patients[14,17,18]; therefore, the diagnostic accuracy of liver strain remains to be assessed in a representative patient population with a range of fibrosis stages.

The aim of this study was to evaluate the diagnostic performance of MRI cine-tagging of cardiac-induced motion for staging liver fibrosis in patients with CLD, using liver biopsy as the reference standard. The secondary aim was to evaluate the influence of potential confounders (i.e., inflammation and steatosis) on strain measurements.

Materials and Methods

Study Design and Subjects

In this prospective ancillary study to a clinical trial (ClinicalTrials.gov Identifier #NCT02044523), 76 patients with clinical suspicion of liver fibrosis were evaluated. This study was approved by the Institutional Review Board of the two participating institutions, Centre hospitalier de l'Université de Montréal and McGill University Health Centre. All subjects provided written informed consent. The prior report, a cross-sectional prospective trial, compared the diagnostic accuracy of US- and MR-based elastography techniques using liver biopsy as the reference standard.[20] In this companion article, MRI cine-tagging sequences were analyzed to evaluate strain as a surrogate of liver elasticity and to evaluate the diagnostic accuracy of these strain measurements for the staging of liver fibrosis. MRI cine-tagging examinations were conducted within 6 weeks of the liver biopsy for all patients, and if performed after the liver biopsy, a minimum delay of 48 hours was observed.

Participants were recruited at the hepatology clinics of the two participating institutions between September 2014 and September 2018. Subjects were included in the study if they were adults who underwent a liver biopsy as part of their clinical standard of care for suspected or known CLD caused by hepatitis B virus (HBV, $n = 2$), hepatitis C virus (HCV, $n = 17$), NAFLD ($n = 7$), nonalcoholic steatohepatitis (NASH, $n = 28$), autoimmune hepatitis (AIH, $n = 16$), or mixed causes ($n = 6$).

Subjects were excluded if they had any contraindication to MRI or if they were unable or unwilling to provide written informed consent for this study. No healthy controls were included. Subjects who met the eligibility criteria were informed of the study's objectives and diagnostic procedures, and, if interested, were given an appointment for an MRI examination. Consecutive potentially eligible participants were included.

Cine-Tagging Experiments

MRI examinations were performed in fasting state with a 3.0T clinical MRI system (Achieva TX, Philips Healthcare, Best, Netherlands). Patients were in the supine position and a 16-channel thoracic surface coil was used. For each patient, a 2D multislice gradient-echo sequence with tagging was acquired with peripheral pulse-wave triggering. Tagging was performed with the spatial modulation of magnetization (SPAMM) preparation sequence, which creates a modulation of the underlying image by a sinusoidal magnetization pattern. The following parameters were used: repetition time (TR), 4.9 msec; echo time (TE), 2.8 msec; flip angle, 10°; field of view, 420 × 420 mm^2; in-plane resolution, 1.3 × 1.3 mm; slice thickness, 8 mm; gap, 16 mm; tag spacing, 8 mm; tag orientation, 0 and 90°; receiver bandwidth, 430 Hz/pixel; SENSE acceleration factor, 2; and number of averages, 1. Depending on the patient's heart rate, 12–15 phases of the cardiac cycle were imaged. Coronal slices at the level of the heart apex were chosen to capture maximal deformation. Images were acquired with two consecutive breath-holds (one per slice) at end-expiration. The total acquisition time was ~16 seconds per slice and was dependent on the patients' cardiac frequency. Measures of iron (R2*) were also performed in the same examination.

MRI Cine-Tagging Postprocessing

The image postprocessing was completed using publicly available HARP software (HARP v. 2.1 for MATLAB, Johns Hopkins University, Baltimore, MD; http://iacl.ece.jhu.edu/index.php/Resources#HARP).[19] The HARP technique was selected for its fast and user-independent analysis of tagged images in order to calculate strain at each point in the image. The sinusoidal modulation of the image in the real domain produces harmonic peaks in the k-space, providing both magnitude

and phase information about the liver. These peaks appear in the k_x and k_y directions on both sides of the central DC peak at the tag pattern frequencies, as seen in Fig. 1b. This is a result of taking the Fourier transform of a sine function that is represented by the sine modulation in both dimensions of the real image. Harmonic images are constructed by applying a bandpass filter on one of the off-centered harmonic peaks in the k-space, and by zero-padding the surrounding space. Filtered harmonic peaks have magnitude and phase components. The phase of the image corresponding to the selected harmonic peak is a material property of the tissue, therefore constant through time,[19] making the measurement of tissue motion and strain through the cardiac cycle possible. Hence, HARP images allow tracking motion of every point in the 2D map.[21] The resulting displacement information allows the calculation of the Eulerian strain tensor at every point. Strain is defined as the variation in length of a material compared with its initial length and is therefore unitless or often expressed as a percentage of deformation. Cardiac-induced deformation of the liver was evaluated over the whole cardiac cycle, using every acquired timeframe.

The maximal amount of stretching, known as the first principal strain P1, or the larger eigenvalue of the 2D Eulerian strain tensor, was examined on two coronal slices. A maximal projection of strain over all timeframes was obtained. A region of interest (ROI) in the liver was identified on each coronal slice as the 2200 mm^2 area within an 80 mm radius of a manually selected point inside the myocardium corresponding to the point of highest cardiac deformation in the apex. This area was obtained by automatically selecting pixels inside this ROI with maximal P1 values on the maximal strain projection map, adding up to 2200 mm^2. P1 values on the two slices were averaged to obtain the average strain in the ROI, which is referred to as strain throughout this article. The computation time was reported for the evaluation of 2D Eulerian strain tensors in the whole segmented liver on the two coronal slices using all timeframes and for the complete evaluation of reported strain values in the ROI close to the heart, including the evaluation of the ROI itself. Timing calculations were performed with MATLAB (R2018a, MathWorks, Natick, MA) on an Intel Core i5-4570 3.20 GHz processor and 2.0 GB of RAM.

Image Analysis

A radiology resident performed the liver segmentation for each subject and manually selected the point corresponding to the highest cardiac deformation in the apex on the time series of tagged MR images. This point was used to obtain the ROI inside the segmented liver. On a random subset of 30 subjects, a second reader with 13 years of experience in radiology (A.T.) performed liver segmentations and the selection of the point inside the apex of the heart to asses the interreader variability.
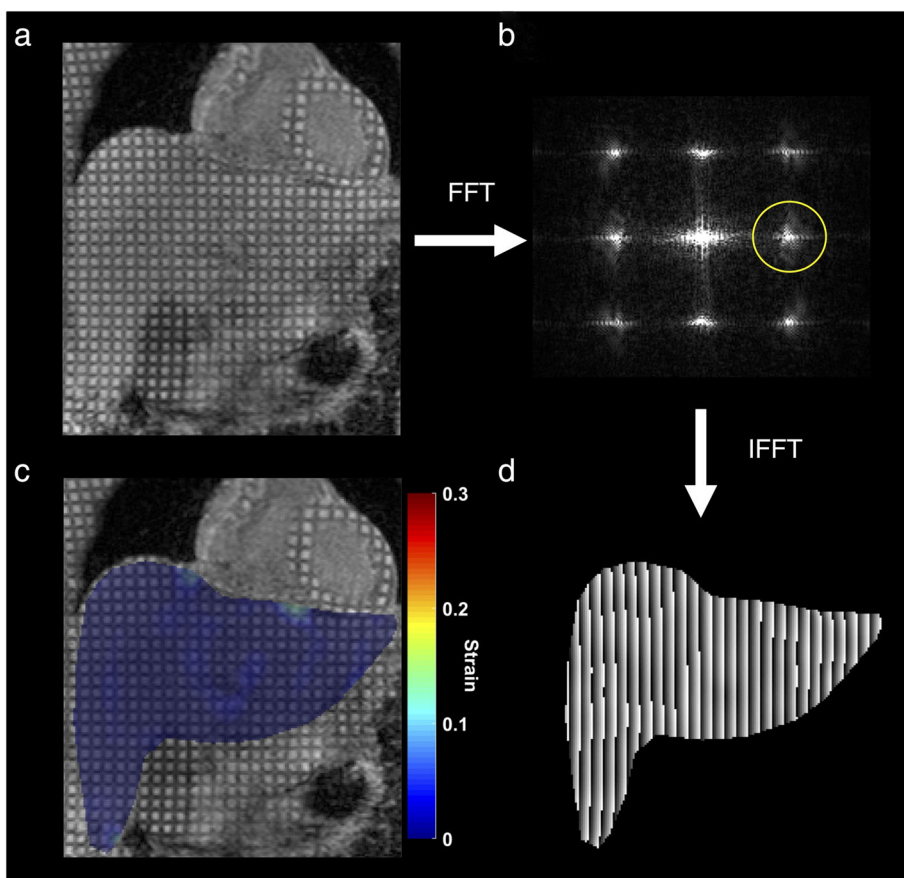

FIGURE 1: (a) MR image with 2D SPAMM grid. (b) Fourier transform of the image with bandpass filter on the first harmonic peak of vertical tags. (c) Tagged MR image with overlaid strain map. (d) Phase image obtained from the inverse Fourier transform of the filtered peak.

Histopathologic Analysis

Liver biopsy was performed in the right lobe by percutaneous approach with 16-G or 18-G core needles. The histology slides of the two participating institutions were interpreted centrally at the Centre hospitalier de l'Université de Montréal by a liver pathologist with 21 years of experience in pathology (B.N.N.). Hematoxylin and eosin slides were assessed for staging of fibrosis, inflammation, and steatosis grades. Fibrosis stages were evaluated on an ordinal scale of F0 to F4, according to the extent and distribution of fibrosis, as well as the degree of architectural remodeling. Inflammation was graded on an ordinal scale of A0 to A3, according to inflammation severity. Steatosis was graded conforming to the proportion of hepatocytes with macrovesicles of fat (using the ordinal scale: S0 is <5%, 1 is 5–33%, S2 is between <33–66%, and S3 is >66%).[22,23] The scoring of histopathological features was performed according to the METAVIR scoring system for patients with HBV, HCV, or AIH (n = 35), and according to the NASH Clinical Research Network scoring system for patients with NASH or NAFLD (n = 35). Histology slides from subjects with mixed causes of CLD were assessed using the scoring system associated with the dominant cause of CLD (n = 7).

Blinding

The image analyst was blinded to the pathology results. The pathologist was blinded to strain measurements and other imaging experiments.

Statistical Analysis

Statistical analyses were performed by a biostatistician with 10 years of experience (M.P.S.) using SAS 9.4 (SAS Institute, Cary, NC) and R 3.4.2 (R Foundation, Vienna, Austria). The intraclass correlation coefficient (ICC) and the within-subject coefficient of variation (CV) were used to assess the interreader variability in a subset of subjects. CV was evaluated as the ratio of the standard deviation of the differences between two strain values to the mean of all strain values. Reproducibility was defined as poor (ICC < 0.4), good (0.4 < ICC < 0.75), or excellent (ICC > 0.75) and a CV value close to zero suggested good agreement between two strain measurements.

The correlation between strain values and liver fibrosis stages was assessed by Spearman's rho (ρ). The nonparametric Kruskal–Wallis rank sum test was performed to compare strain values between all fibrosis stages. Pairwise comparisons between fibrosis stages were performed with a post hoc Mann–Whitney U-test with Bonferroni correction for multiple comparisons. A univariate analysis was also performed to assess the correlation between strain and inflammation, and between strain and steatosis, using Spearman's analysis. A multiple regression analysis was performed to explore the confounding effects of inflammation and steatosis on the association between fibrosis and liver strain. Estimated regression coefficients and estimated standardized regression coefficients are reported. The significance level for all statistical analyses was defined as $P < 0.05$. Dichotomized groups of hepatic fibrosis stages were used to evaluate the discriminatory capability of cardiac-induced strain measurements as follows: F0 vs. ≥ F1, ≤ F1 vs. ≥ F2; ≤ F2 vs. ≥ F3; and ≤ F3 vs. F4. The diagnostic performance of strain for staging liver fibrosis was assessed with the receiver operating characteristic (ROC) analysis. The area under the ROC curve (AUC) was reported for each dichotomization of fibrosis stages and for distinguishing stage F0 from F4 in order to compare it with results from prior studies. Sensitivity, specificity, accuracy, positive predictive value (PPV), and negative predictive value (NPV) were evaluated for thresholds, resulting in a sensitivity approaching 90%. Bootstrapping by resampling data 1000 times was used to compute the 95% confidence intervals (CI).

Results

The study population comprised 76 eligible patients who underwent MRI and liver biopsy during the recruitment period (September 2014 to September 2018) (Fig. 2). Half of the population were women (n = 38) and the population mean age was 53 years (range: 20–76 years) (Table 1).

Histopathological findings were distributed as follows in our cohort: for fibrosis stage, 8 (10%) patients had F0 fibrosis, 15 (20%) F1, 19 (25%) F2, 12 (16%) F3, and 22 (29%)
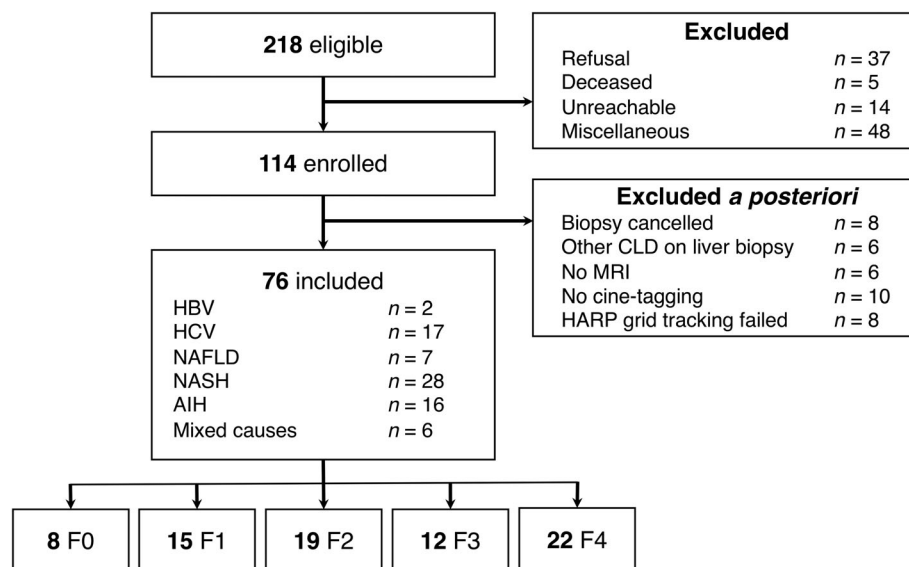

FIGURE 2: Flowchart of patient selection.

TABLE 1. Characteristics in 76 Patients	
Characteristic	**Data**
Sex	
Male	38 (50%)
Female	38 (50%)
Age (y)	
Mean $\pm$ SD (range)	53 $\pm$ 12 (20–76)
BMI (kg/m^2)	
Mean $\pm$ SD (range)	29.0 $\pm$ 5.9 (17–47)
< 25	20 (26%)
$\geq$ 25 and < 30	21 (28%)
$\geq$ 30 and < 40	32 (42%)
$\geq$ 40	3 (4%)
Diabetes	24 (32%)
Hypertension	30 (39%)
Laboratory tests: Mean $\pm$ SD (range)	
AST (U/L)	55 $\pm$ 50 (14–319)
ALT (U/L)	79 $\pm$ 84 (13–473)
GGT (U/L)	89 $\pm$ 93 (12–464)
Platelet count (x 10^9/L)	201 $\pm$ 62 (94–383)
Total bilirubin (µmol/L)	12.8 $\pm$ 5.4 (4.5–29.0)
Prothrombin time (%)	99.8 $\pm$ 8.2 (83–120)
Alkaline phosphatase (U/L)	67 $\pm$ 49 (16–249)
Albumin (g/L)	40.5 $\pm$ 6.6 (31–79)
Cholesterol (mmol/L)	4.5 $\pm$ 1.0 (2.9–7.0)
Biopsy length (mm)	
Mean $\pm$ SD (range)	18.5 $\pm$ 6.4 (7–30)
Fibrosis stage	
F0 (none)	8 (10%)
F1 (perisinusoidal or periportal)	15 (20%)
F2 (periportal and presence of septa)	19 (25%)
F3 (numerous septa without cirrhosis)	12 (16%)
F4 (cirrhosis)	22 (29%)
Inflammation activity grade	
A0 (none)	5 (7%)

| TABLE 1. Continued	
Characteristic	**Data**
A1 (negligible)	38 (50%)
A2 (moderate)	25 (33%)
A3 (severe)	8 (10%)
Steatosis grade	
S0 (<5% hepatocytes involved)	32 (42%)
S1 (5%-33% hepatocytes involved)	19 (25%)
S2 (33%-66% hepatocytes involved)	12 (16%)
S3 (>66% hepatocytes involved)	13 (17%)

Numbers in parentheses are percentages, unless otherwise specified. SD = standard deviation, BMI = body mass index, AST = aspartate aminotransferase, ALT = alanine aminotransferase, GGT = gamma-glutamyl transpeptidase.

F4; for inflammation activity grade, 5 (7%) patients had grade A0, 38 (50%) grade A1, 25 (33%) grade A2, and 8 (10%) grade A3; for steatosis grade, 32 (42%) patients had grade S0, 19 (25%) grade S1, 12 (16%) grade S2, and 13 (17%) grade S3. The time interval between MRI and biopsy never exceeded 6 weeks (range: 1 day to 6 weeks).

In the included subjects, mean R2* was 53.4 $\pm$ 12.4 s^{-1} (32.3–96.6 s^{-1}). HARP tracking could not be performed successfully in eight eligible subjects who were excluded a posteriori from the study population (Fig. 2). Mean R2* in this group was 116.1 $\pm$ 46.7 s^{-1} (70.2–220.0 s^{-1}).

Mean liver strain measured by MRI cine-tagging of cardiac-induced motion was 0.12 $\pm$ 0.06 (standard deviation) for the patient group of fibrosis stage F0, 0.08 $\pm$ 0.02 for stage F1, 0.07 $\pm$ 0.04 for stage F2, 0.06 $\pm$ 0.01 for stage F3, and 0.04 $\pm$ 0.01 for stage F4. Figure 3 shows representative maximal intensity projection maps and strain maps at the timeframe of maximal deformation for each fibrosis stage. In our cohort, the mean calculation time of 2D Eulerian strain tensors in the whole segmented liver on the two coronal slices using all timeframes was 1.18 $\pm$ 0.20 s (0.70–1.82 s). The mean time for evaluating the reported strain values in the ROI close to the heart was 8.50 $\pm$ 3.10 s (2.70–16.56 s). In a subset of patients (n = 30), the distance between the point selected in the apex of the heart by the two readers was 1.2 $\pm$ 0.6 cm (0.2–2.6 cm) on average. The ICC and CV for strain values obtained in the ROI resulting from the segmentation of the two readers were 0.584 and 29.7%, respectively.
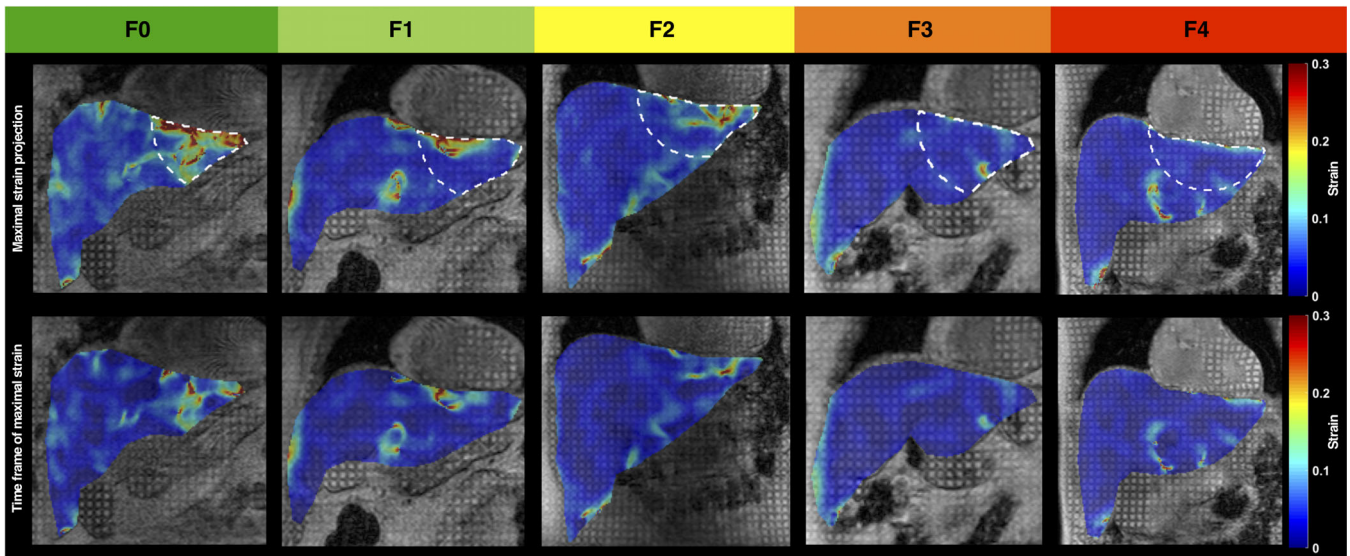
FIGURE 3: Maximal strain projection maps and strain maps overlaid on tagged MR images at the timeframe of maximal strain in patients with liver fibrosis stages F0 to F4 as assessed by liver biopsy. ROIs were limited to a 2200 mm² area within a radius of 80 mm from the manually selected point inside the myocardium near the apex, as shown by the white dashed line. Subjects with fibrosis stages F0, F1, F2, F3, and F4 had cardiac-induced liver strain of 0.13, 0.08, 0.07, 0.04, and 0.03, respectively.

A significant and negative correlation was obtained between liver strain and fibrosis stages (ρ = –0.68, $P < 0.0001$). The Kruskal–Wallis rank sum test showed that liver strain was significantly different across all histologically determined fibrosis stages ($P < 0.0001$). For dichotomized groups of fibrosis stages, Mann–Whitney U-tests demonstrated that only the distinction of fibrosis groups ≤F3 vs. F4 was significant ($P < 0.05$). Boxplots showing the range of liver strain associated with fibrosis stages are shown in Fig. 4.

In univariate analysis, a significant and negative correlation was obtained between liver strain and inflammatory activity grades (ρ = –0.28, $P < 0.05$), while no significant correlation was obtained between liver strain and steatosis grades (ρ = 0.11, $P = 0.37$). Hence, only fibrosis stages and inflammation grades were included in the multiple regression analysis model. The confounding effect of inflammation on association between fibrosis and liver strain was not significant. In fact, inflammation was not significantly associated with liver strain in the multiple regression analysis (Table 2). Estimated standardized regression coefficients were –0.61 ($P < 0.0001$) for fibrosis and –0.09 ($P = 0.38$) for inflammation. Scatterplots of liver strain on association with inflammation and steatosis are shown in Fig. 5.

Estimates of diagnostic performance for detecting fibrosis stages using liver strain measured from tagged MRI are shown in Table 3 and ROC curves in Fig. 6. Area under the ROC curves (AUC) were 0.95 (95% bootstrapped CI: 0.89–1.00) with a threshold of 0.065 for distinguishing fibrosis stages F0 vs. F4, 0.81 (0.70–0.92) with a threshold of 0.095 for stages F0 vs. ≥ F1, 0.84 (0.76–0.93) with a threshold of 0.086 for stages ≤ F1 vs. ≥ F2, 0.86 (0.78–0.94) with a threshold of 0.063 for stages ≤ F2 vs. ≥ F3, and 0.87 (0.77–0.96) with a threshold of 0.061 for stages ≤ F3 vs. F4.

Discussion

This prospective ancillary study evaluated MRI cine-tagging for measurement of liver strain for noninvasive liver fibrosis staging in patients with CLD, using histopathology as the reference standard. Liver strain was calculated by analyzing SPAMM-tagged images with the HARP method in an ROI close to the heart apex in the left liver lobe. Liver biopsy specimens were read by an experienced hepatopathologist.
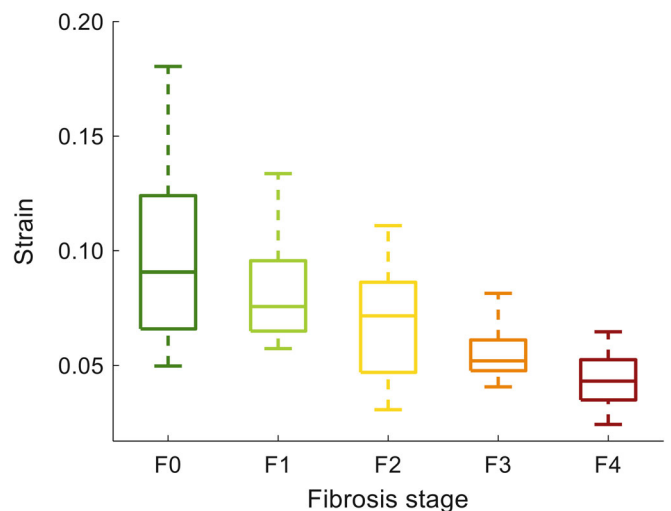
FIGURE 4: Median liver strain with interquartile ranges vs. fibrosis stages. Mean liver strain in our population was 0.12 ± 0.06 for subjects with fibrosis stage F0, 0.08 ± 0.02 for stage F1, 0.07 ± 0.04 for stage F2, 0.06 ± 0.01 for stage F3, and 0.04 ± 0.01 for stage F4. Strain values were significantly different between all fibrosis stages ($P < 0.0001$). The median is represented by the band in the box; the box indicates the first and third quartile, and whiskers indicate the minimum and maximum values.

TABLE 2. Univariate Analysis and Multiple Regression Analysis of Liver Fibrosis, Inflammation, and Steatosis Impact on Strain

	Univariate analysis		Multiple regression analysis				
	ρ	P	Estimated coefficients	Standard deviation	Estimated standardized coefficients	P	Adjusted R^2
Fibrosis	−0.68	< 0.0001	−0.013	0.002	-0.61	< 0.0001	
Inflammation	−0.28	< 0.05	−0.003	0.004	-0.09	0.38	0.41
Steatosis	0.11	0.37					

Strain measurements had good reproducibility, with some variability in a random subset of subjects. We found that liver strain decreased with increasing fibrosis stage. There was a strong correlation between fibrosis stages and liver strain in univariate analysis, which also yielded a significant correlation for discriminating between fibrosis stages. The diagnostic performance given by the threshold resulting in a sensitivity approaching 90% for distinguishing subjects between dichotomized fibrosis stages were also derived. Additionally, potential confounders (i.e., inflammation and steatosis) did not significantly affect the correlation between liver strain and hepatic fibrosis stages in our cohort.

Previous studies used smaller sample sizes[14,17,18] or compared healthy volunteers to cirrhotic patients.[14,15,17] Some had larger cohorts but used the aspartate aminotransferase to platelet ratio index score[16] or the Child-Pugh score[15] as a surrogate reference standard. Strengths of this study included the larger sample size, broader spectrum of fibrosis stages, and reliance on the accepted "gold standard" for liver fibrosis staging, i.e., histopathological analysis of a liver biopsy specimen.

Fibrosis has been shown to alter the mechanical properties of the liver, such as elasticity and viscosity. US- and MR-based techniques report values for these properties, which are indicative of liver stiffness. Previous studies have shown the correlation between these techniques and fibrosis stages, and their ability to classify stages.[24–27] The increase in stiffness is due to the accumulation of extracellular matrix proteins specific to fibrosis.[28,29] In this study, the mechanical deformation of the liver, or strain, was assessed. Strain is related to the stiffness of the tissue, reflecting its elasticity and viscosity. Liver strain reflects the change in shape or size of the liver that occurs when a force is applied. Liver stiffness, as measured with MRE, for instance, indicates the tendency of the liver to return to its original shape or size after being subjected to a force, hence how it resists elastic deformation when a force is applied.[30] A stiffer tissue will undergo less strain; hence, fibrotic or cirrhotic livers will tend to move as a whole instead of being deformed by the action of the heart. This explains the negative relationship between fibrosis stage and strain.
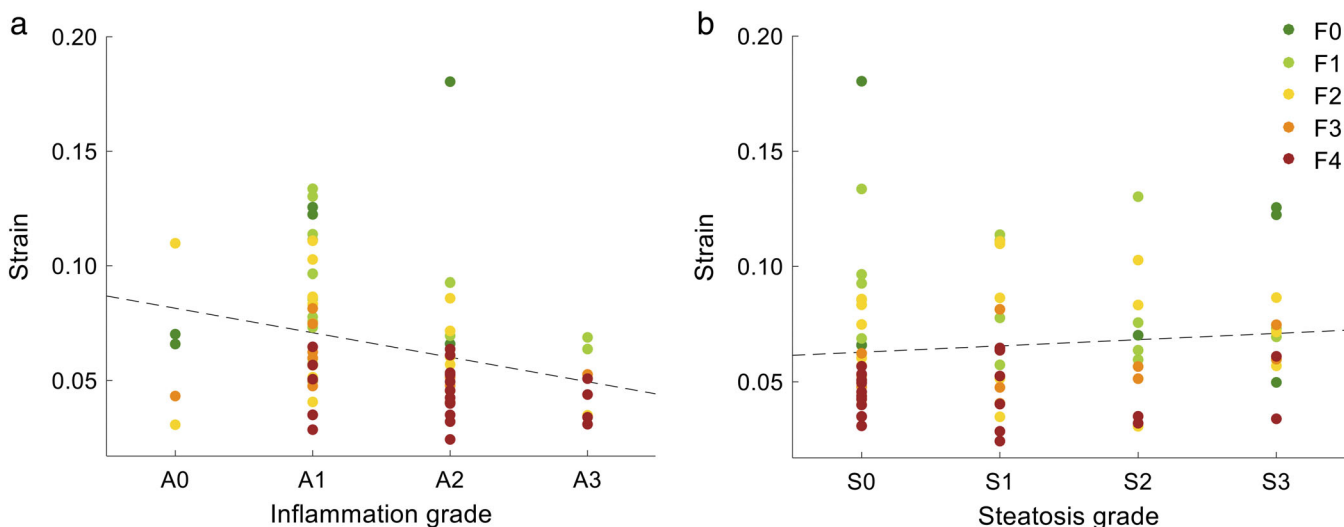
FIGURE 5: Scatterplots of liver strain as a function of histology-determined (a) inflammation grade and (b) steatosis grade. Dashed lines correspond to linear regressions

TABLE 3. Diagnostic Performance of Strain Measured by MRI Cine-Tagging of Cardiac-Induced Motion for Staging Liver Fibrosis (95% CI in Parentheses)

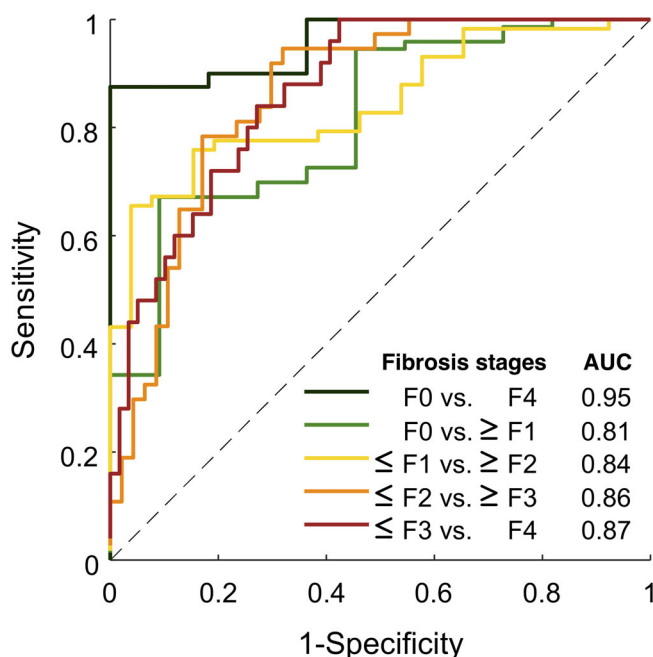| Fibrosis stage	AUC	Threshold	Sensitivity (%)	Specificity (%)	Accuracy (%)	PPV(%)	NPV(%)
F0 (n = 8) vs.F4 (n = 22)	0.95(0.89–1.00)	0.065	88(73–98)	100(85–100)	96(78–100)	100(84–100)	96(79–100)
F0 (n = 8) vs.≥ F1 (n = 68)	0.81(0.70–0.92)	0.095	89(80–95)	55(23–83)	85(75–91)	93(84–98)	43(18–71)
≤ F1 (n = 23) vs.≥ F2 (n = 53)	0.84(0.76–0.93)	0.086	90(79–96)	42(23–63)	75(64–84)	78(66–87)	65(38–86)
≤ F2 (n = 42) vs.≥ F3 (n = 34)	0.86(0.78–0.94)	0.063	89(75–97)	70(55–83)	79(68–87)	70(55–83)	89(75–97)
≤ F3 (n = 54) vs. F4 (n = 22)	0.87(0.77–0.96)	0.061	88(69–97)	61(47–73)	70(58–79)	49(34–64)	92(79–98)

Data in parentheses are raw. AUC = area under the ROC curve, PPV = positive predictive value, NPV = negative predictive value.

In univariate analysis, we found that liver strain also decreased with inflammation, to a lesser degree. Inflammation has been reported to increase the liver's stiffness, hence to decrease the liver's capacity to be stretched in patients with CLD.[31–33] However, the impact of inflammation on strain was not significant in multiple regression analysis. The impact on steatosis was not significant in univariate analysis. Fat deposition might decrease the liver's stiffness when using elastography techniques employing a high frequency range,

FIGURE 6: Receiver operating characteristic curves of liver strain for distinguishing dichotomized groups of fibrosis stages.

such as US-based shear wave elastography.[34] However, at the low heartbeat frequency, fat was not found to confound strain measurements in this study.

We did not expect a perfect correlation between fibrosis stages and liver strain. In fact, many factors were not considered in our assessment. One source of disparity could be that heart motion consists of a complex 3D movement of torsion and contraction that is not solely located in the coronal plane. A coaxial plane could provide a more comprehensive evaluation of the liver's deformation from cardiac motion. Most previous studies reported strain values averaged over three coronal planes and three sagittal planes, using ROIs of 314 mm^2 or 324 mm^2.[14–17] In our study, using two different depths in the coronal plane provided a compact representation of how cardiac motion compresses the left lobe of the liver. Future work could evaluate the optimal number of slices to acquire for simulating a time-efficient 3D reconstruction of the liver to measure cardiac-induced liver strain. Such studies have already been undertaken, performing 3D MRE of the liver with high diagnostic accuracy for staging liver fibrosis.[35]

A total acquisition time of about 16 seconds per slice, depending on the patient's cardiac frequency, is highly comparable to the acquisition time of MRE, but without the need for an external driver to generate mechanical waves.[36] Hence, it would be feasible to implement this fast, although not real-time technique, clinically on screening abdominal MRI, especially considering that strain evaluated on two coronal slices provided good accuracy for staging liver fibrosis. For post-processing, it took less than 2 seconds to generate strain values for all acquired timeframes on the two coronal slices and less than 10 seconds on average to generate strain values

from the ROI as described above. ROI definition could be optimized by simply using elliptical ROIs manually positioned in the left liver close to the heart apex, similar to the clinical measurement approach for MRE.[36]

We reported the average strain on a maximal strain projection map in a larger area than previous studies (2200 mm^2 vs. 314 mm^2 or 324 mm^2).[14–17] We assumed that averaging maximal strain in a larger area would be more representative of the overall liver strain and that this maximal strain evaluated within a radius of 80 mm from the heart apex was necessarily coming from cardiac-induced deformation. In fact, using strain values from a maximal strain projection map in a region close to the heart was deemed accurate to avoid confounding effects of neighboring organs' movement on strain. However, the generated strain maps demonstrate higher strain values in small areas close to the heart and may thus be vulnerable to sampling and strain heterogeneity. Good reproducibility was obtained but some variability was still present from one reading to another, suggesting that the ROI selection might have an impact on the resulting strain value. The current work represents a proof-of-concept, rather than a presentation of a clinical-grade software. Hence, future work should analyze and compare the reliability of various ROI methods.

We found that liver strain measured by MRI cine-tagging provided good AUCs for the diagnosis of liver fibrosis stage F1 or higher, stage F2 or higher, stage F3 or higher, and stage F4 (cirrhosis). While the sensitivity was intentionally high, approaching 90% by design, the specificity was low or moderate. Because of its minimal acquisition time, we envisioned this MRI technique as a screening or surveillance tool for *detection* of liver fibrosis, hence the emphasis on high sensitivity. If a patient has a suspicion of clinically significant fibrosis (stage F2 or higher), we would recommend further investigation by MRE or liver biopsy if a formal diagnosis is warranted.

In our MRI cine-tagging study, the AUC ranged from 0.81, 0.84, 0.86, and 0.87 for staging of liver fibrosis F0 vs. ≥ F1, ≤ F1 vs. ≥ F2, ≤ F2 vs. ≥ F3, ≤ F3 vs. F4. This compares favorably with AUCs reported for MRE in subjects with CLD or NAFLD, which reported AUCs ranging from 0.84–0.86, 0.87–0.88, 0.90–0.93, and 0.91–0.92, respectively.[24,37]

Our results differed in some ways from previously reported MRI cine-tagging studies. Watanabe et al found that AUCs for staging histology-confirmed liver fibrosis with bending energy analysis on 16-mm tagged sagittal images were 0.798, 0.802, 0.471, and 0.629 for F0 vs. ≥ F1, ≤ F1 vs. ≥ F2, ≤ F2 vs. ≥ F3, ≤ F3 vs. F4, respectively.[13] Watanabe et al evaluated bending energy on sagittal slices, whereas we evaluated strain on coronal slices. Hence, although AUCs were higher in our study, especially for staging advanced stages of fibrosis, thresholds used for staging fibrosis cannot be directly compared. Chung et al reported AUCs of 0.995

for distinguishing healthy subjects from cirrhotic subjects with a Child-Pugh score A or higher, and of 0.891 for distinguishing healthy subjects from cirrhotic subjects with a Child-Pugh score B or higher, using maximal strain across three coronal and three sagittal planes in one ROI of 324 mm^2.[15] Although the technique is similar to ours, their selection of subjects at opposite ends of the disease spectrum (healthy subjects vs. cirrhotic patients) explains the good performance reported in their study. A similar AUC was obtained in our population for distinguishing fibrosis stage F0 from F4 (0.95), which resembles their analysis more closely. The mean strain reported for their control group was similar to that of our subjects, with F0 (0.10 ± 0.02 vs. 0.12 ± 0.06). The mean strain in their group with Child-Pugh score A or higher was the same as the one found in our group of subjects with F4 (0.04 ± 0.01 vs. 0.04 ± 0.01). Manelli et al also reported very similar mean strain in an 80 mm^2 ROI in the left liver lobe underneath the heart in a group of patients with cirrhosis (0.04 ± 0.03), but ROC analysis was not performed.[17]

HARP grid tracking failed in some subjects due to tags fading. The mean R2*, a biomarker of liver iron concentration, was higher among subjects with HARP grid tracking failure than among included patients. The presence of iron overload has been shown to shorten T_2* and T_1 relaxation times,[38] which are associated with the tag pattern duration. Hence, higher liver iron concentration may lead to earlier fading and HARP tracking failure. Because the average liver iron concentration was relatively low in our study population, the HARP algorithm could be used successfully in most subjects to evaluate strain from MRI cine-tagging of cardiac-induced motion at 3.0T. However, in a population with high iron overload incidence, higher rates of failure could be observed, as the HARP algorithm can be sensitive to noise and tag fading in the image.[39]

The main limitations of the current study are the following. Differences in subjects' myocardial strain and blood pressure need to be considered to assess fibrosis stage relative to patients' heart condition. Future studies may acquire tagged coaxial slices of the heart to evaluate myocardial strain according to clinically available methods in order to normalize liver strain.[40] The heterogeneity of our population is another limitation. Although it reflects the clinical reality where patients with suspected CLD or multiple coexisting causes of CLD are screened, it might also have introduced variability in the reported results. Another source of disparity could arise from the fact that biopsy samples were obtained in the right liver lobe while strain measurements were performed in the left liver lobe in a region close to the heart apex. As fibrosis is a heterogeneous disease, stages assessed from samples from the right lobe might not reflect the stage that would have been obtained from samples coming from the left lobe. In fact, the left lobe is generally smaller than the right lobe and is therefore covered by more capsule per unit area. As subcapsular

portal tracts tend to be more fibrous than deeper portal tracts within the liver parenchyma, this could change the assessment of the fibrosis stage, depending on if the biopsy sample originated from the left or the right liver lobe.[41] The small sampling size of biopsy is also an issue when staging fibrosis stage within the same lobe with other noninvasive techniques. Other liver biopsy limitations have already been stated in the literature.[42] Hence, high correlation between strain measurements and fibrosis stages was not expected and confirms that there might be a difference in fibrosis distribution within the left lobe compared with the right lobe. Therefore, there is an interest in noninvasively evaluating fibrosis in the left liver lobe. Other US-based and MR-based elastographic methods mostly assess the right liver and, as the transducer is typically placed above that liver side, the left lobe may be more difficult to assess. Thus, MRI cine-tagging could be used as a complementary technique to evaluate the stiffness of the left liver lobe.

In conclusion, in a cohort of subjects with suspected or known CLD, this cross-sectional study demonstrated the relationship between liver strain and histologically determined, centrally scored fibrosis stages. Movements and deformations of the liver induced by cardiac motion were measured using tagged images. These images were analyzed with the HARP method and the extracted strain values were found to allow classification of dichotomized fibrosis stages. MRI cine-tagging is understood to be a promising technique for measuring liver strain without additional elastography hardware. Additional studies are required to validate its use in clinical care and compare its liver fibrosis staging accuracy with MRE.

References

1. Tsochatzis EA, Bosch J, Burroughs AK. Liver cirrhosis. Lancet 2014;383: 1749–1761.

2. Sebastiani G, Gkouvatsos K, Pantopoulos K. Chronic hepatitis C and liver fibrosis. World J Gastroenterol 2014;20:11033–11053.

3. Blachier M, Leleu H, Peck-Radosavljevic M, Valla DC, Roudot-Thoraval F. The burden of liver disease in Europe: A review of available epidemiological data. J Hepatol 2013;58:593–608.

4. Estes C, Razavi H, Loomba R, Younossi Z, Sanyal AJ. Modeling the epidemic of nonalcoholic fatty liver disease demonstrates an exponential increase in burden of disease. Hepatology 2018;67:123–133.

5. Bedossa P, Carrat F. Liver biopsy: The best, not the gold standard. J Hepatol 2009;50:1–3.

6. Kennedy P, Wagner M, Castera L, et al. Quantitative elastography methods in liver disease: Current evidence and future directions. Radiology 2018;286:738–763.

7. Castera L, Foucher J, Bernard PH, et al. Pitfalls of liver stiffness measurement: A 5-year prospective study of 13,369 examinations. Hepatology 2010;51:828–835.

8. Tang A, Cloutier G, Szeverenyi NM, Sirlin CB. Ultrasound elastography and MR elastography for assessing liver fibrosis: Part 2. Diagnostic performance, confounders, and future directions. AJR Am J Roentgenol 2015;205:33–40.

9. Venkatesh SK, Ehman RL. Magnetic resonance elastography of abdomen. Abdom Imaging 2015;40:745–759.

10. Wagner M, Corcuera-Solano I, Lo G, et al. Technical failure of MR elastography examinations of the liver: Experience from a large single-center study. Radiology 2017;284:401–412.

11. Venkatesh SK, Ehman RL. Magnetic resonance elastography of liver. Magn Reson Imaging Clin N Am 2014;22:433–446.

12. Zerhouni EA, Parish DM, Rogers WJ, Yang A, Shapiro EP. Human heart: Tagging with MR imaging—A method for noninvasive assessment of myocardial motion. Radiology 1988;169:59–63.

13. Watanabe H, Kanematsu M, Kitagawa T, et al. MR elastography of the liver at 3 T with cine-tagging and bending energy analysis: Preliminary results. Eur Radiol 2010;20:2381–2389.

14. Chung S, Breton E, Mannelli L, Axel L. Liver stiffness assessment by tagged MRI of cardiac-induced liver motion. Magn Reson Med 2011; 65:949–955.

15. Chung S, Kim KE, Park MS, Bhagavatula S, Babb J, Axel L. Liver stiffness assessment with tagged MRI of cardiac-induced liver motion in cirrhosis patients. J Magn Reson Imaging 2014;39:1301–1307.

16. Kim KE, Park MS, Chung S, An C, Axel L, Ergashovna RG. Magnetization-tagged MRI is a simple method for predicting liver fibrosis. Clin Mol Hepatol 2016;22:140–145.

17. Mannelli L, Wilson GJ, Dubinsky TJ, et al. Assessment of the liver strain among cirrhotic and normal livers using tagged MRI. J Magn Reson Imaging 2012;36:1490–1495.

18. Harouni AA, Gharib AM, Osman NF, Morse C, Heller T, Abd-Elmoniem KZ. Assessment of liver fibrosis using fast strain-encoded MRI driven by inherent cardiac motion. Magn Reson Med 2015;74:106–114.

19. Osman NF, Kerwin WS, McVeigh ER, Prince JL. Cardiac motion tracking using CINE harmonic phase (HARP) magnetic resonance imaging. Magn Reson Med 1999;42:1048–1060.

20. Lefebvre T, Wartelle-Bladou C, Wong P, et al. Prospective comparison of transient, point shear wave, and magnetic resonance elastography for staging liver fibrosis. Eur Radiol 2019 [Epub ahead of print].

21. Liu X, Prince JL. Shortest path refinement for motion estimation from tagged MR images. IEEE Trans Med Imaging 2010;29:1560–1572.

22. Kleiner DE, Brunt EM, Van Natta M, et al. Design and validation of a histological scoring system for nonalcoholic fatty liver disease. Hepatology 2005;41:1313–1321.

23. Bedossa P, Poynard T. An algorithm for the grading of activity in chronic hepatitis C. The METAVIR Cooperative Study Group. Hepatology 1996;24:289–293.

24. Singh S, Venkatesh SK, Wang Z, et al. Diagnostic performance of magnetic resonance elastography in staging liver fibrosis: A systematic review and meta-analysis of individual participant data. Clin Gastroenterol Hepatol 2015;13:440–451 e446.

25. Nierhoff J, Chavez Ortiz AA, Herrmann E, Zeuzem S, Friedrich-Rust M. The efficiency of acoustic radiation force impulse imaging for the staging of liver fibrosis: A meta-analysis. Eur Radiol 2013;23:3040–3053.

26. Friedrich-Rust M, Ong MF, Martens S, et al. Performance of transient elastography for the staging of liver fibrosis: A meta-analysis. Gastroenterology 2008;134:960–974.

27. Herrmann E, de Ledinghen V, Cassinotto C, et al. Assessment of biopsy-proven liver fibrosis by two-dimensional shear wave elastography: An individual patient data-based meta-analysis. Hepatology 2018;67:260–272.

28. Bataller R, Brenner DA. Liver fibrosis. J Clin Invest 2005;115:209–218.

29. Wells RG. The role of matrix stiffness in hepatic stellate cell activation and liver fibrosis. J Clin Gastroenterol 2005;39(4 Suppl 2):S158–161.

30. Petitclerc L, Sebastiani G, Gilbert G, Cloutier G, Tang A. Liver fibrosis: Review of current imaging and MRI quantification techniques. J Magn Reson Imaging 2017;45:1276–1295.

31. Chen J, Talwalkar JA, Yin M, Glaser KJ, Sanderson SO, Ehman RL. Early detection of nonalcoholic steatohepatitis in patients with nonalcoholic fatty liver disease by using MR elastography. Radiology 2011;259:749–756.

32. Yin M, Glaser KJ, Talwalkar JA, Chen J, Manduca A, Ehman RL. Hepatic MR elastography: Clinical performance in a series of 1377 consecutive examinations. Radiology 2016;278:114–124.

33. Hartl J, Denzer U, Ehlken H, et al. Transient elastography in autoimmune hepatitis: Timing determines the impact of inflammation and fibrosis. J Hepatol 2016;65:769–775.

34. Kazemirad S, Zhang E, Nguyen BN, et al. Detection of steatohepatitis in a rat model by using spectroscopic shear-wave US elastography. Radiology 2016:160308.

35. Loomba R, Cui J, Wolfson T, et al. Novel 3D magnetic resonance elastography for the noninvasive diagnosis of advanced fibrosis in NAFLD: A prospective study. Am J Gastroenterol 2016;111:986–994.

36. Venkatesh SK, Yin M, Ehman RL. Magnetic resonance elastography of liver: Technique, analysis, and clinical applications. J Magn Reson Imaging 2013;37:544–555.

37. Singh S, Venkatesh SK, Loomba R, et al. Magnetic resonance elastography for staging liver fibrosis in non-alcoholic fatty liver disease: A diagnostic accuracy systematic review and individual participant data pooled analysis. Eur Radiol 2016;26:1431–1440.

38. Hernando D, Levin YS, Sirlin CB, Reeder SB. Quantification of liver iron with MRI: State of the art and remaining challenges. J Magn Reson Imaging 2014;40:1003–1021.

39. Arts T, Prinzen FW, Delhaas T, Milles JR, Rossi AC, Clarysse P. Mapping displacement and deformation of the heart with local sine-wave modeling. IEEE Trans Med Imaging 2010;29:1114–1123.

40. Chitiboi T, Axel L. Magnetic resonance imaging of myocardial strain: A review of current approaches. J Magn Reson Imaging 2017;46:1263–1280.

41. Brunt EM, Tiniakos DG. Histopathology of nonalcoholic fatty liver disease. World J Gastroenterol 2010;16:5286–5296.

42. Bedossa P, Dargere D, Paradis V. Sampling variability of liver fibrosis in chronic hepatitis C. Hepatology 2003;38:1449–1457.